Journal of Asian Earth Sciences 34 (2009) 674–685

Contents lists available at ScienceDirect

Journal of Asian Earth Sciences

journal homepage: www.elsevier.com/locate/jaes

$^{40}Ar/^{39}Ar$ dating of the Jiali and Gaoligong shear zones: Implications for crustal deformation around the Eastern Himalayan Syntaxis

Te-Hsien Lin [a], Ching-Hua Lo [a,*], Sun-Lin Chung [a], Fang-Jui Hsu [a], Meng-Wan Yeh [b], Tung-Yi Lee [b], Jian-Qing Ji [c], Yi-Zhau Wang [d], Dunyi Liu [e]

[a] Department of Geosciences, National Taiwan University, No. 1, Sec. 4, Roosevelt Road, Taipei 10617, Taiwan
[b] Department of Earth Sciences, National Taiwan Normal University, Taipei, Taiwan
[c] School of Earth and Space Science, Peking University, Beijing, China
[d] Regional Geological Survey Party, Yunnan Bureau of Geology and Mineral Exploration and Development, China
[e] Institute of Geology, Chinese Academy of Geological Sciences, Beijing, China

ARTICLE INFO

Article history:
Received 28 May 2008
Received in revised form
26 September 2008
Accepted 3 October 2008

Keywords:
$^{40}Ar/^{39}Ar$ dating
Shear zone
Eastern Himalayan Syntaxis
Tibet

ABSTRACT

We conducted a comprehensive $^{40}Ar/^{39}Ar$ geochronological study of the Jiali and Gaoligong shear zones to obtain a better understanding of crustal deformation and tectonic evolution around the Eastern Himalayan Syntaxis (EHS). The new age data reveal that the main phase of deformation in the Jiali and Gaoligong shear zones occurred from 22 to 11 Ma and from 18 to 13 Ma, respectively. Structural data collected during this study indicate that the Jiali shear zone underwent a change in shear sense from sinistral to dextral during its movement history. Based on a comparison with the deformation histories of other major shear zones in the region, we argue that the initial sinistral motion recorded by the Jiali shear zone was coincident with that of the Ailao Shan–Red River shear zone, which marked the northern boundary of the southeastward extrusion of the Indochina block during the Early Miocene. From the Middle Miocene (~18 Ma), the Jiali shear zone changed to dextral displacement, becoming linked with the dextral Gaoligong shear zone that developed as a consequence of continued northward indentation of the Indian continent into Asia. Since this time, the Jiali and Gaoligong shear zones have been united, defining the southwestern boundary of the EHS during clockwise rotation of the eastward-extruding Tibetan block, as revealed by recent GPS data. The temporal change in regional deformation pattern from southeastward block extrusion to clockwise rotation of crustal fragments may have played an important role in the development of the eastern Himalayan drainage system around the EHS.

1. Introduction

In response to shortening associated with collision between the Indian and Eurasian plates, lithospheric material of the Tibetan Plateau and adjacent foreland regions has undergone significant intracontinental deformation. Various models and hypotheses have been proposed to explain the kinematic and tectonic processes associated with formation of the Tibetan Plateau and plate-scale deformation in East Asia. Among them, the indentation–extrusion model proposed by Tapponnier et al. (1982) has been widely discussed. This model proposes that a large component of convergence was accommodated by the extrusion of continental fragments along the main lithospheric-scale strike-slip faults of the region; however, recent GPS and geodetic data have revealed significant clockwise block rotation around the Eastern Himalayan Syntaxis (EHS) along several N–S-trending shear zones (Fig. 1) rather than the eastward extrusion of the South China block predicted by the indentation–extrusion model (Chen et al., 2000; Wang et al., 2001; Zhang et al., 2004).

In recent decades, many thermochronological studies conducted in the region of the Tibetan Plateau have focused on metamorphic complexes and syntectonic magmatic events (Lacassin et al., 1997; Wang et al., 1998; Bertrand et al., 2001; Lee et al., 2003) with the aim of constraining the timing and amount of displacement, and rate of movement along shear zones and during block rotation (Fig. 1). For example, Wang et al. (1998, 2000) reported sinistral shear along the Ailao Shan-Red River (ASRR) shear zone at 27–17 Ma. Armijo et al. (1989) proposed that the dextral Jiali shear zone and dextral–reverse ASRR shear zone linked up to form the southern boundary of the eastward-extruded northern Tibet and South China regions following the southeastward extrusion of Indochina. However, the Early Miocene (18–12 Ma; Lee et al., 2003) deformation recorded along the Jiali shear zone has yet to be reported from the ASRR shear zone, and the dextral Sagaing Fault, which has previously been proposed as the western

* Corresponding author. Tel.: +886 2 3366 2915; fax: +886 2 2363 6095.
E-mail address: loch@ntu.edu.tw (C.-H. Lo).

1367-9120/$ - see front matter © 2008 Elsevier Ltd. All rights reserved.
doi:10.1016/j.jseaes.2008.10.009

boundary of southeastward-extruded Indochina, did not become active until ca. 22 Ma (Searle et al., 2007).

GPS-based velocity studies (Chen et al., 2000; Wang et al., 2001; Zhang et al., 2004) reveal that present-day deformation is concentrated upon several N–S-trending shear zones (the Jiali, Gaoligong, and Sagaing shear zones in the west, and the Xianshuihe, Xiaojiang, and Dien Bien Phu faults in the east) around the EHS (Burchfiel, 2004; Fig. 1). Although these recent geodetic studies highlight the important role of the shear zones in the tectonic evolution of Southeast Asia, they have received little attention in terms of geochronological analyses. In the present study, we carried out U–Pb and $^{40}Ar/^{39}Ar$ dating on samples of leucogranite, gneiss, and mylonite collected along the Jiali and Gaoligong shear zones, with the aim of constraining (i) the tectonic evolution of the region around the EHS, and (ii) the deformation of continental blocks in response to India–Asia collision.

2. Geological background

The E–W-trending dextral Jiali shear zone extends from about 30°42′N, 92°50′E, where it intersects the northern tip of a WNW–ESE-trending normal fault system in southern Tibet, toward the EHS. The shear zone splays into two major branches (the Poqu and Parlung faults) toward its southeastern end, where it cuts the easternmost part of the Gangdese Batholith (Fig. 1) (Molnar and Tapponnier, 1978; Ni and York, 1978; Armijo et al., 1989; Lee et al., 2003). The Parlung and Poqu faults are thought to extend further southward into Yunnan and Burma to join the Gaoligong and Sagaing shear zones, respectively (Fig. 1) (Armijo et al., 1989; Wang and Burchfiel, 1997).

Based on focal mechanism analyses of the Chayu earthquake (M = 8.7) of 15 August 1950, the Jiali shear zone is thought to accommodate dextral strike-slip displacement with a component

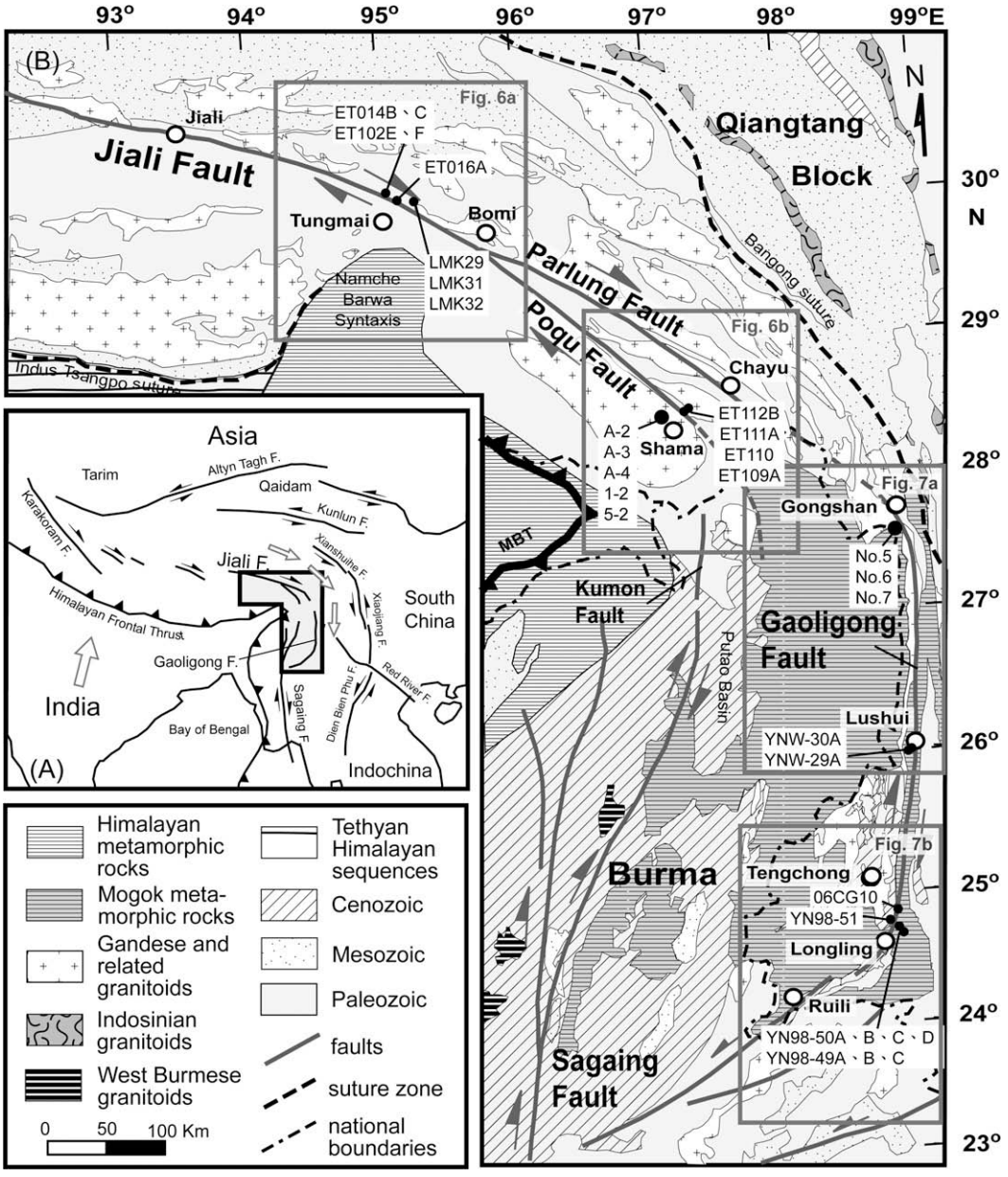

Fig. 1. (A) Topographic map showing the main active faults in Tibet and adjacent regions. White arrows indicate the directions of present-day plate motions. (B) Simplified geological map of the study area (modified from Lee et al., 2003). Solid circles indicate sample localities. Gray arrows indicate shear sense along shear zones, as determined from GPS data (Chen et al., 2000; Wang et al., 2001; Zhang et al., 2004).

of thrusting (Molnar and Deng, 1984); however, shear sense indicators observed in oriented thin sections (e.g., matrix foliations and shear-band cleavages) indicate an earlier sinistral displacement. These findings indicate that the shear zone was initially sinistral, but was later reactivated with the present-day dextral movement (Fig. 2a and b; M.-W. Yeh, unpublished data). A previous thermochronological study of sheared granitic rocks from Shama and Chayu reported that following the attainment of peak metamorphic conditions (estimated to be $\geqslant$500 °C and ~3–5 kbar), shearing along the Poqu and Parlung faults occurred during the Early Miocene, at 12–18 Ma (Fig. 1) (Lee et al., 2003).

The northern Gaoligong shear zone lies within and along the margin of the N–S-trending Gaoligong Mountain belt, western Yunnan, China, where metamorphic rocks are thrust over Silurian to Early Cretaceous strata (Fig. 1; Wang and Burchfiel, 1997). The trend of the southern Gaoligong shear zone changes to NE–SW around Longling, where high-grade metamorphic rocks are thrust over strata as young as Late Cretaceous (Fig. 1; Wang and Burchfiel, 1997). Geodetic and structural data (Fig. 2c) reveal a combination of dextral shearing and thrusting along the Gaoligong shear zone (Wang and Burchfiel, 1997; M.-W. Yeh, unpublished data).

We analyzed a sample of mylonite from the Gongshan area (sample No. 5) with the aim of estimating the peak metamorphic conditions within the Gaoligong shear zone. The sample, which contains the assemblage garnet + sillimanite + biotite + K-feldspar + plagioclase + quartz, was analyzed for mineral chemistry

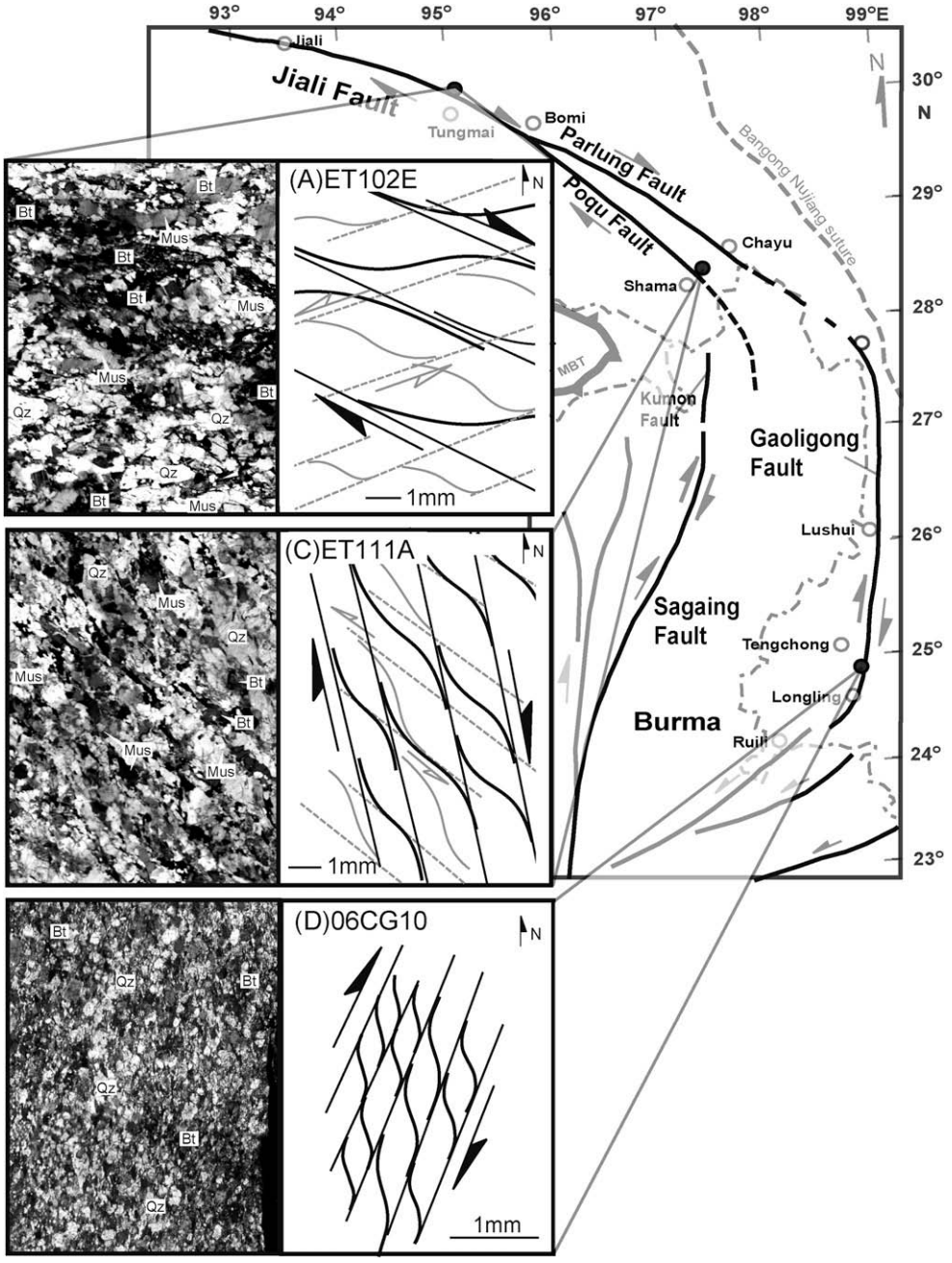

Fig. 2. Photomicrographs and accompanying line diagrams showing textural relations and relative timing of events. All photomicrographs were taken from horizontal, oriented thin sections, with arrows indicating shear sense. (A) Contrasting shear senses recorded in samples from the Tungmai area. An early foliation that records sinistral deformation (fine lines with white arrows indicating shear sense) was overprinted by a foliation that records dextral deformation (thick lines with black arrows indicating shear sense). (B) Contrasting shear senses in a sample collected from the Shama area. (C) Dextral shear sense recorded in a sample collected from the Gaoligong shear zone between the Tengcheng and Longling areas.

Table 1
Mineral compositions for sample No. 5 from the Gaoligong shear zone in Gongshan area.

Mineral (weight per cent oxides)	SiO_2	TiO_2	Al_2O_3	Cr_2O_3	FeO	MnO	MgO	CaO	Na_2O	K_2O	P_2O_5	Total
Garnet	38.53	0.00	21.98	0.05	34.73	2.13	4.32	1.01	0.00	0.00	0.13	102.89
	38.60	0.00	22.06	0.03	35.46	2.15	3.80	1.05	0.00	0.01	0.07	103.23
	38.22	0.04	21.89	0.03	34.13	2.28	4.07	1.13	0.01	0.01	0.05	101.87
	38.59	0.00	22.17	0.02	34.76	2.57	3.71	1.13	0.02	0.02	0.13	103.12
	36.00	0.00	22.23	0.05	35.36	3.08	2.74	1.10	0.00	0.02	0.02	100.58
	38.20	0.05	22.08	0.00	35.14	3.14	2.96	1.09	0.00	0.02	0.09	102.76
Average	38.02	0.02	22.07	0.03	34.93	2.56	3.60	1.08	0.01	0.01	0.08	102.41
Biotite	36.11	2.49	18.94	0.12	19.12	0.14	10.16	0.00	0.10	9.60	0.04	96.82
	35.63	2.47	18.80	0.06	19.03	0.13	9.74	0.00	0.12	9.78	0.04	95.80
	36.20	2.21	19.18	0.07	18.50	0.08	9.70	0.03	0.07	9.82	0.06	95.93
	36.18	2.24	19.01	0.00	17.91	0.13	9.63	0.00	0.06	9.84	0.02	95.01
	35.54	3.60	18.82	0.05	20.09	0.16	9.34	0.00	0.10	9.71	0.01	97.42
	35.13	3.69	17.08	0.00	19.89	0.17	9.08	0.00	0.07	9.74	0.00	94.85
Average	35.80	2.78	18.64	0.05	19.09	0.14	9.61	0.00	0.09	9.75	0.03	95.97

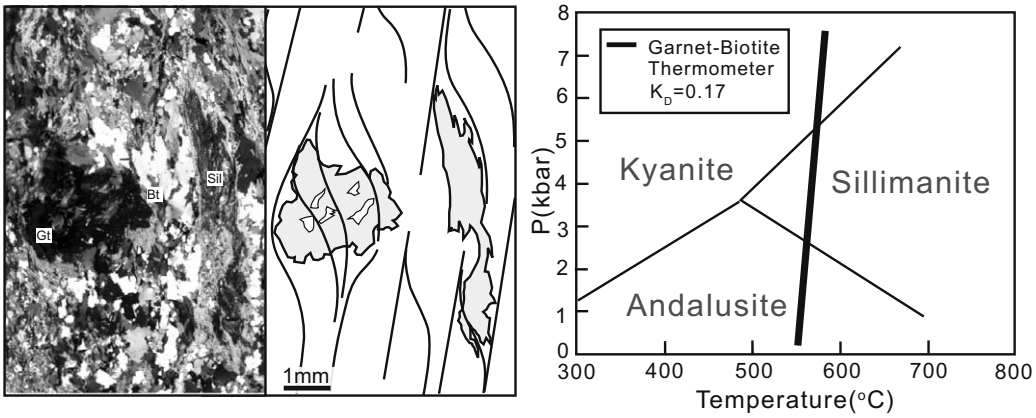

Fig. 3. (A) Photomicrograph of sample No. 5 (mylonite), showing a mineral assemblage of garnet + sillimanite + biotite + K-feldspar + plagioclase + quartz. (B) P–T diagram, showing the K_D = 0.17 line obtained using a garnet–biotite geothermometer. The stability fields of andalusite, kyanite, and sillimanite are from Holdaway (1971). Gt = garnet, Sil = sillimanite, Bt = biotite.

using a JEOL JXA-8900R electron microprobe housed at Academia Sinica, Taiwan. Garnet porphyroblasts contain curved inclusion tails continuous with the matrix foliation and are bordered by strain shadows. The matrix foliation is deflected around porphyroblasts, indicating syn- or inter-tectonic growth. Using the garnet–biotite geothermometer of Hodges and Spear (1982), we obtained metamorphic conditions of around 550 °C and 3–5 kbar (Table 1; Fig. 3) for the Gaoligong shear zone, consistent with previous estimates for the southern segment of the zone (Zhong et al., 1991).

Previous K–Ar dating of mylonite within the Gaoligong shear zone has yielded ages of 11.6–23.8 Ma (Zhong et al., 1991), consistent with ages derived from micas in the Sagaing shear zone (15.8–26.9 Ma; Bertrand et al., 2001) is coincidence led Ding and Zhong (1992) to suggest that the Gaoligong shear zone is a northern extension of the Sagaing shear zone. Combining field observations, paleomagnetic data, and age data, Wang and Burchfiel (1997) further proposed that clockwise rotation of continental blocks along these shear zones around the EHS commenced during the Early Neogene.

3. Analytical methods

Zircon separates from two rock samples (sample ET014B: a leucogranite from the Tungmai-Bomi area; sample A-3: a mylonite from the Chayu-Shama area) collected from the Jiali shear zone (Fig. 1) were analyzed by SHRIMP at the Beijing SHRIMP Center, Institute of Geology, Chinese Academy of Geological Sciences. Details of the analytical procedure can be found in Chu et al. (2006). The analyzed zircons are mostly euhedral and prismatic, ranging in length from ~150 to 200 μm. Mineral grains are transparent, colorless to slightly brown, and show oscillatory zoning typical of magmatic growth. Sample ET014B showing magmatic features associated with sheared fabrics, is considered as a syn- or pre-kinematic intrusion. Thus, the obtained zircon U–Pb age, which represents the crystallization age of the sample, is interpreted to indicate the timing of shearing in the Tungmai-Bomi area. The zircon U–Pb age obtained for sample A-3 (mylonite) represents the crystallization age of the protolith, providing a maximum age for deformation in the Chayu-Sharma area.

$^{40}Ar/^{39}Ar$ single-grain fusion methods, using a laser heating technique, were applied to muscovite and biotite separates extracted from mylonitic gneiss and pegmatite and aplite veins from the Jiali and Gaoligong shear zones (Fig. 1; Table 3). The pegmatite and aplite veins appear to follow the foliation within the host gneiss and mylonite, and are therefore interpreted as products of shearing deformation. Rock samples were first crushed and then sieved. Mineral grains of the 140–250 μm fraction were ultrasonically cleaned in distilled water and dried. Muscovite and biotite were then handpicked under a microscope. Mineral separates and a neutron flux monitor (LP-6 biotite; Odin et al., 1982) were irradiated in the VT-C position at the Tsing-Hua Open-Pool Reactor (THOR), Taiwan, for 30 h. After irradiation, samples and the moni-

Table 2
SHRIMP U–Pb data of zircon separates from sample A-3 and ET014B.

Spot	Th/U	U–Th–Pb ratios								Ages (Ma)						Inferred age (Ma)	1σ
		$^{206}Pb/^{238}U$	1σ	$^{207}Pb/^{206}Pb$	1σ	$^{207}Pb/^{235}U$	1σ	$^{208}Pb/^{232}Th$	1σ	$^{206}Pb/^{238}U$	1σ	$^{207}Pb/^{206}Pb$	1σ	$^{208}Pb/^{232}Th$	1σ		
A-3 (mylonite)																	
A-3-02.1	0.41	0.0034	0.0001	0.0894	0.0119	0.0413	0.0056	0.0019	0.0002	21.6	0.5	1413.8	255.3	38.0	4.3	21.6	0.5
A-3-03.1	0.27	0.0033	0.0001	0.0534	0.0018	0.0243	0.0010	0.0011	0.0001	21.3	0.4	343.8	77.7	22.2	1.4	21.3	0.4
A-3-06.1	0.17	0.0032	0.0001	0.0498	0.0018	0.0218	0.0009	0.0011	0.0001	20.5	0.4	184.0	82.9	22.8	1.6	20.5	0.4
A-3-08.1	0.08	0.0032	0.0001	0.0478	0.0015	0.0208	0.0007	0.0010	0.0001	20.4	0.4	87.0	72.1	20.2	2.6	20.4	0.4
A-3-09.1	0.25	0.0032	0.0001	0.0583	0.0042	0.0259	0.0020	0.0013	0.0001	20.8	0.6	539.9	158.0	27.2	2.9	20.8	0.6
A-3-10.1	0.15	0.0031	0.0001	0.0510	0.0007	0.0219	0.0005	0.0011	0.0000	20.1	0.4	238.8	33.7	22.6	0.9	20.1	0.4
A-3-11.1	0.68	0.0033	0.0001	0.0477	0.0017	0.0219	0.0009	0.0011	0.0000	21.4	0.4	85.6	85.2	22.0	0.6	21.4	0.4
A-3-12.1	0.19	0.0032	0.0001	0.0567	0.0019	0.0249	0.0010	0.0017	0.0000	20.5	0.4	479.2	75.6	33.4	1.3	20.5	0.4
A-3-13.1	0.39	0.0031	0.0001	0.0609	0.0026	0.0264	0.0012	0.0013	0.0000	20.2	0.4	636.7	91.6	26.6	1.0	20.2	0.4
A-3-14.1	0.46	0.0032	0.0001	0.0534	0.0032	0.0236	0.0015	0.0011	0.0001	20.6	0.5	347.9	137.2	23.2	1.3	20.6	0.5
A-3-16.1	0.61	0.0034	0.0001	0.0512	0.0010	0.0243	0.0007	0.0011	0.0000	22.1	0.5	251.8	44.2	23.1	0.6	22.1	0.5
ET014B (leucogranite)																	
ET014B-01.1	0.21	0.0034	0.0001	0.0410	0.0143	0.0351	0.0040	0.0008	0.0005	22.1	0.6	1039.4	223.3	43.4	6.2	22.1	0.6
ET014B-02.1	0.23	0.0037	0.0001	0.0468	0.0185	0.0589	0.0082	0.0008	0.0005	23.6	0.6	1902.0	244.5	71.5	10.9	23.6	0.6
ET014B-03.1	0.30	0.0036	0.0001	0.0371	0.0227	0.0369	0.0048	0.0007	0.0006	23.3	0.5	1038.5	256.6	36.0	4.9	23.3	0.5
ET014B-04.1	0.31	0.0036	0.0001	0.0408	0.0256	0.0405	0.0048	0.0009	0.0007	23.1	0.6	1240.0	228.7	41.6	5.1	23.1	0.6
ET014B-05.1	0.35	0.0035	0.0001	0.0328	0.0427	0.0344	0.0026	0.0007	0.0010	22.5	0.5	965.8	146.6	34.2	3.6	22.5	0.5
ET014B-06.1	0.24	0.0036	0.0001	0.0241	0.0239	0.0291	0.0069	0.0004	0.0008	23.1	0.6	555.7	517.7	33.2	7.6	23.1	0.6
ET014B-07.1	0.22	0.0037	0.0001	0.0376	0.0200	0.0414	0.0057	0.0009	0.0007	23.7	0.6	1231.2	267.1	55.7	6.2	23.7	0.6
ET014B-09.1	0.22	0.0036	0.0001	0.0281	0.0280	0.0310	0.0068	0.0005	0.0010	22.9	0.6	713.1	465.4	37.8	10.2	22.9	0.6
ET014B-10.1	0.26	0.0035	0.0001	0.0535	0.0619	0.0411	0.0046	0.0014	0.0020	22.7	0.5	1308.8	212.0	49.5	6.5	22.7	0.5
ET014B-11.1	0.24	0.0036	0.0001	0.0391	0.0207	0.0357	0.0049	0.0003	0.0007	23.0	0.5	1001.7	272.6	31.2	4.3	23.0	0.5
ET014B-14.1	0.21	0.0038	0.0001	0.0684	0.0352	0.0526	0.0068	0.0022	0.0015	24.8	0.5	1608.3	236.9	74.5	10.7	24.8	0.5
ET014B-15.1	0.27	0.0037	0.0001	0.0270	0.0323	0.0373	0.0113	0.0007	0.0009	23.9	0.7	1010.0	609.8	46.2	11.7	23.9	0.7
ET014B-16.1	0.19	0.0037	0.0001	0.0657	0.0207	0.0616	0.0099	0.0026	0.0005	24.0	0.6	1955.3	283.6	108.7	15.7	24.0	0.6

tor minerals were degassed using a Nd-YAG laser operated in continuous mode. Argon isotopes were measured using a VG3600 mass spectrometer housed at the National Taiwan University, Taiwan. *J* values were calculated using the argon composition of the LP-6 biotite monitor, with a calibrated $^{40}Ar/^{39}Ar$ age of 128.4 ± 0.2 Ma based on Fish Canyon Sanidine (28.02 ± 0.28 Ma; Renne et al., 1998). Ages are calculated from Ar isotopic ratios measured after correction for mass discrimination, interfering nuclear reactions, procedural blanks, and atmospheric Ar contamination. Details of the procedures followed for isotope analyses and age calculations can be found in Lo et al. (2002).

4. Results

The zircon U–Pb dating results of two samples (ET014B and A-3) are summarized in Table 2, and shown in Fig. 4 by U–Pb concordia diagrams. The results of $^{40}Ar/^{39}Ar$ analyses are summarized in Table 3 and available in the depository data set. The results of laser single-grain fusion analyses are plotted in $^{36}Ar/^{40}Ar$ versus $^{39}Ar/^{40}Ar$ isotope correlation diagrams, from which intercept ages and $^{40}Ar/^{36}Ar$ initial values were obtained by regression of the data (Table 3; Figs. 5–7). In all cases, the age results form linear arrays with reasonable mean square of weighted deviation (MSWD; 0.689–3.389), and $^{40}Ar/^{36}Ar$ initial ratios (268–328) are in general agreement with the atmospheric ratio (295.5). These findings indicate negligible excess argon or thermal disturbance in the samples, and that the Ar in the samples is mainly composed of radiogenic and atmospheric components. In addition, the ages appear to show a single mode and small standard deviation for individual samples. The intercept ages are comparable with the mean ages (Fig. 5). We therefore interpret the intercept ages to represent the metamorphic and cooling ages of the dated samples.

4.1. Jiali shear zone

SHRIMP analyses of 14 zircon grains in sample ET014B yield U–Pb ages of 22–26 Ma, with a weighted mean age of 22.2 ± 0.4 (2σ) Ma (MSWD = 0.73; Table 2; Fig. 4). Eleven zircon grains from sample A-3 yield similar U–Pb zircon ages of 20–22 Ma, with a weighted mean age of 20.6 ± 0.4 (2σ) Ma (MSWD = 1.81; Table 2; Fig. 4). The U and Th concentrations in samples ET014B and A-3 fall in the ranges of 446–9442 and 105–5749 ppm, respectively; most zircons have Th/U values of >0.1. Given that the obtained U–Pb zircon ages are relatively young, and that zircons with rounded or ovoid shapes and complex internal textures are rare, the obtained weighted means of pooled $^{206}Pb/^{238}U$ ages are taken to represent the crystallization ages of the host rocks.

Given that the peak metamorphic temperatures estimated for the Jiali and Gaoligong shear zones (~550 °C) are higher than the mica Ar isotopic closure temperature, all the mica dates are interpreted to record cooling ages. Single-grain analyses for biotites from five samples (ET014C, ET016A, LMK32, LMK31, and LMK29) from the Jiali shear zone in the Tungmai-Bomi area (Fig. 1) yield $^{40}Ar/^{39}Ar$ ages ranging from 21.3 to 10.9 Ma (1σ of ±0.1–0.3 Ma; Table 3; Fig. 6). Biotite grains from six samples (ET110, 1-2, A-2, 5-2, A-4, and A-3) from the Chayu-Shama area yield $^{40}Ar/^{39}Ar$ ages of 19.9 to 13.7 Ma (1σ of ±0.1–0.4 Ma; Table 3; Fig. 6). Muscovite grains (from samples ET112B, ET110, and ET109A) from the same area yield similar ages, ranging from 18.7 to 11.3 Ma (1σ error of ±0.2–0.5 Ma; Table 3; Fig. 6). The muscovite age obtained for sample ET110 is slightly older than the biotite age, indicating rapid cooling since ~18 Ma.

Overall, the $^{40}Ar/^{39}Ar$ ages obtained for the Jiali shear zone are either comparable with or younger than the U–Pb ages reported above. A comparison of $^{40}Ar/^{39}Ar$ ages reveals that the oldest biotite age for the Chayu-Shama area (19.9 Ma) is younger than that for the Tungmai-Bomi area (21.3 Ma). In summary, the $^{40}Ar/^{39}Ar$ ages for 15 mica separates from the Jiali shear zone range from 21.3 to 10.9 Ma (1σ error of ±0.1–0.5 Ma).

4.2. Gaoligong shear zone

Laser $^{40}Ar/^{39}Ar$ single-grain analyses of three biotite grains (grains No. 5, No. 6, and No. 7) from the Gaoligong shear zone in the Gongshan area yielded ages ranging from 15.5 to 12.8 Ma (1σ error of ±0.3–0.4 Ma; Table 3; Fig. 7). Six biotite grains (YN98-51, YN-98-50A, YN98-50B, YN98-50D, YN98-49A, and YN98-49B) from the Longling area yielded ages ranging from 16.1 to 14.0 Ma (1σ error of ±0.5–0.7 Ma; Table 3; Fig. 7). The muscovite ages of two samples (YN98-50C and YN98-49C) collected from the Longling area are 16.2 and 16.5 Ma, respectively, slightly older than the biotite ages determined for samples from the same outcrops. Biotite grains within samples YNW-30A and

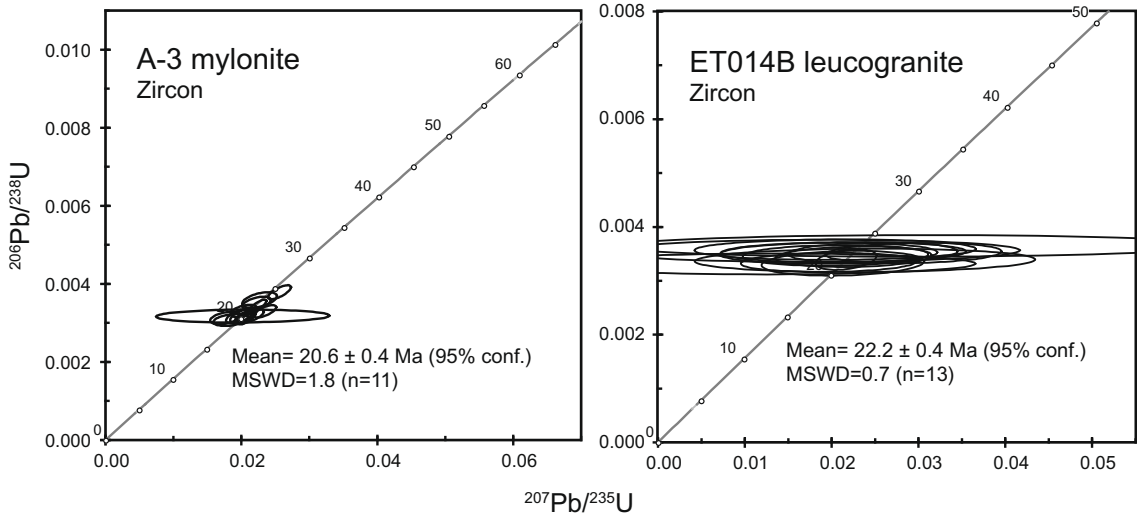

Fig. 4. U–Pb concordia plots for mylonite and leucogranite from the Jiali shear zone.

Table 3
Summary of $^{40}Ar/^{39}Ar$ dating results conducted on micas from metamorphic and intrusive samples collected along the Jiali and Gaoligong shear zones.

	Location	Sample	Rock type	Phase	Latitude (°N)	Longitude (°E)	Mean age (Ma)	Std[a]	Intercept age (Ma)	$(^{40}Ar/^{36}Ar)_i$	MSWD[b]
Jiali shear zone	Tungmai-Bomi	ET014C	gneiss	Biotite	30.11	95.07	21.3 ± 0.7	1.5	21.0 ± 0.1	321 ± 6	2.628
	Tungmai-Bomi	ET016A	gneiss	Biotite	30.07	95.14	10.8 ± 0.2	0.4	10.9 ± 0.1	307 ± 10	2.184
	Tungmai-Bomi	ET102F	gneiss	Biotite	30.10	95.07	21.3 ± 0.2	0.3	21.2 ± 0.3	299 ± 17	1.195
	Tungmai-Bomi	LMK32	mylonite	Biotite	30.06	95.04	15.6 ± 0.1	0.2	15.5 ± 0.1	321 ± 40	0.774
	Tungmai-Bomi	LMK31	mylonite	Biotite	30.04	95.09	15.3 ± 0.2	0.3	15.4 ± 0.1	287 ± 6	2.701
	Tungmai-Bomi	LMK29	mylonite	Biotite	30.02	95.16	14.3 ± 0.2	0.4	14.2 ± 0.1	327 ± 10	0.731
	Chayu-Shama	ET112B	mylonite	Muscovite	28.54	97.09	11.4 ± 0.1	0.2	11.3 ± 0.5	297 ± 6	2.293
	Chayu-Shama	ET110	gneiss	Biotite	28.51	97.07	17.0 ± 0.6	1.2	16.2 ± 0.4	317 ± 6	1.937
	Chayu-Shama	ET110	gneiss	Muscovite	28.51	97.07	18.6 ± 0.2	0.4	18.7 ± 0.2	287 ± 17	1.687
	Chayu-Shama	ET109A	gneiss	Muscovite	28.49	97.06	12.7 ± 0.2	0.4	12.7 ± 0.4	303 ± 8	3.158
	Shama	1-2	mylonite	Biotite	28.27	97.03	13.9 ± 0.3	0.7	13.9 ± 0.1	297 ± 8	2.038
	Shama	A-2	mylonite	Biotite	28.27	97.03	13.7 ± 0.1	0.1	13.7 ± 0.1	277 ± 24	2.095
	Shama	5-2	mylonite	Biotite	28.22	97.02	15.3 ± 0.1	0.2	15.4 ± 0.1	271 ± 31	0.781
	Shama	A-4	mylonite	Biotite	28.22	97.02	19.8 ± 0.3	0.5	19.9 ± 0.2	303 ± 12	1.417
	Shama	A-3	mylonite	Biotite	28.21	97.01	14.5 ± 0.2	0.3	14.5 ± 0.1	315 ± 8	1.796
Gaoligong shear zone	Gongshan	No. 5	mylonite	Biotite	27.65	98.67	13.7 ± 0.1	0.2	13.6 ± 0.3	308 ± 89	0.689
	Gongshan	No. 6	mylonite	Biotite	27.61	98.70	12.7 ± 0.1	0.2	12.8 ± 0.4	287 ± 25	0.939
	Gongshan	No. 7	mylonite	Biotite	27.61	98.62	16.1 ± 0.2	0.4	15.5 ± 0.4	328 ± 14	1.135
	Lushui	YNW-30A	mylonite	Biotite	25.97	98.77	18.3 ± 0.3	0.4	17.9 ± 0.5	360 ± 79	0.730
	Lushui	YNW-29A	mylonite	Biotite	25.96	98.77	17.8 ± 0.1	0.2	17.6 ± 0.5	324 ± 62	1.090
	Longling	YN98-51	mylonite	Biotite	24.85	98.74	13.9 ± 0.3	0.4	14.0 ± 0.5	278 ± 68	0.861
	Longling	YN98-50A	mylonite	Biotite	24.82	98.78	15.0 ± 0.2	0.3	14.7 ± 0.6	313 ± 25	1.531
	Longling	YN98-50B	mylonite	Biotite	24.82	98.78	15.0 ± 0.3	0.6	15.1 ± 0.6	268 ± 68	0.847
	Longling	YN98-50C	aplitic granite	Muscovite	24.82	98.78	16.2 ± 0.2	0.3	16.2 ± 0.7	298 ± 20	1.049
	Longling	YN98-50D	pegmatite	Biotite	24.82	98.78	15.7 ± 0.2	0.3	15.7 ± 0.6	301 ± 24	2.043
	Longling	YN98-49A	mylonite	Biotite	24.80	98.79	15.7 ± 0.5	0.9	16.1 ± 0.7	284 ± 14	3.389
	Longling	YN98-49B	mylonite	Biotite	24.80	98.79	15.4 ± 0.4	0.6	15.6 ± 0.5	291 ± 10	1.601
	Longling	YN98-49C	pegmatite	Muscovite	24.80	98.79	16.4 ± 0.2	0.4	16.5 ± 0.6	286 ± 19	1.532

[a] Std: standard deviation.
[b] MSWD: mean square weighted deviation.

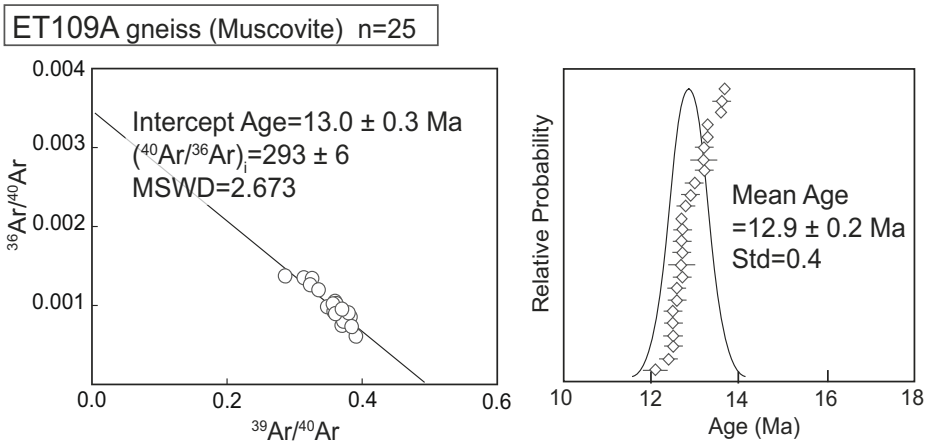

Fig. 5. $^{36}Ar/^{40}Ar$ versus $^{39}Ar/^{40}Ar$ isotope correlation diagram and age probability curve for sample ET109A muscovite. Data are represented by open circles, with ±1σ error ellipses.

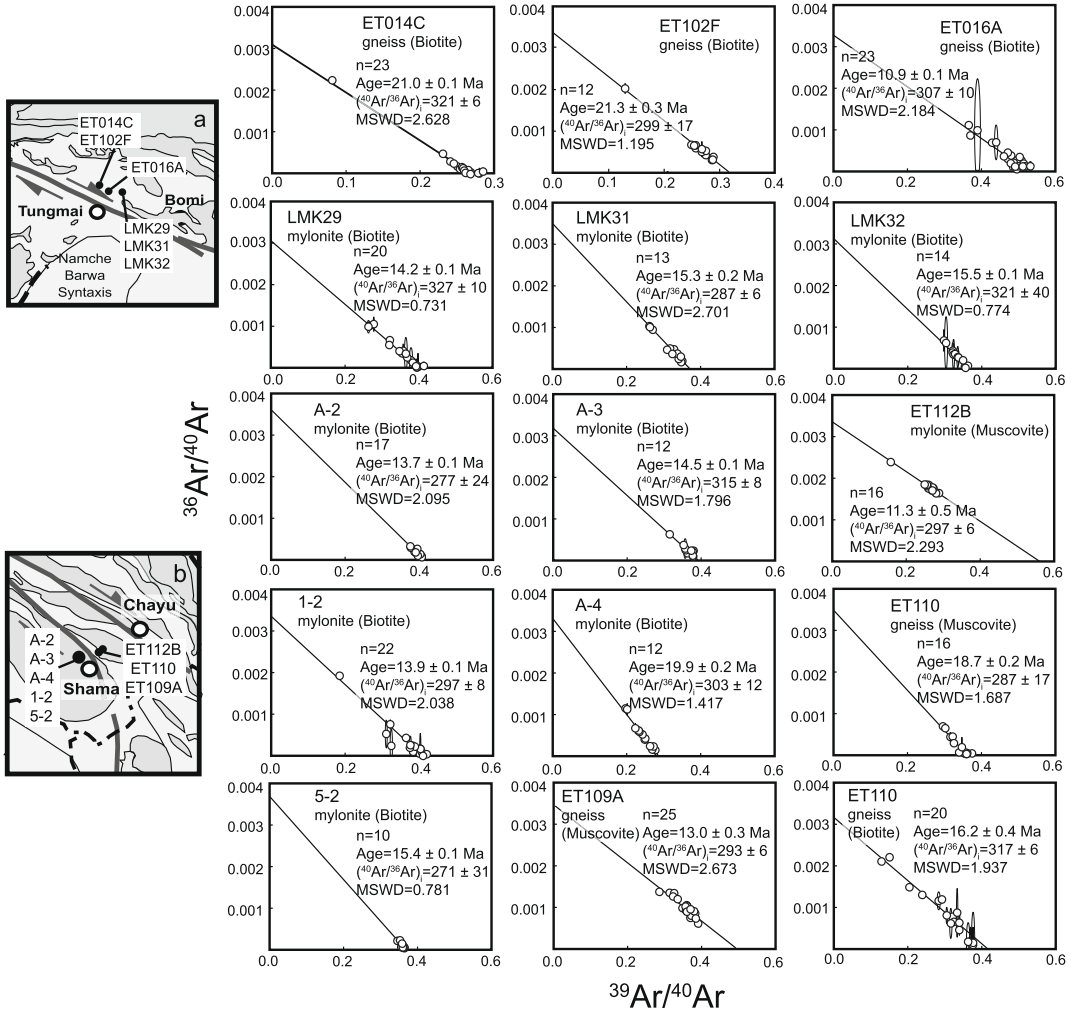

Fig. 6. $^{36}Ar/^{40}Ar$ versus $^{39}Ar/^{40}Ar$ isotope correlation diagrams for samples from the Jiali shear zone. Data are represented by open circles, with ±1σ error ellipses.

YNW-29A in the same shear zone from the Lushui area yielded the oldest $^{40}Ar/^{39}Ar$ ages of 17.9 and 17.5 Ma, respectively (1σ error of ±0.5 Ma; Table 3; Fig. 7).

In summary, analyses of 12 mica samples from the Gaoligong shear zone yield a relatively young and narrow $^{40}Ar/^{39}Ar$ age span of 17.9 to 12.8 Ma (1σ error of ±0.3–0.7 Ma; Table 3).

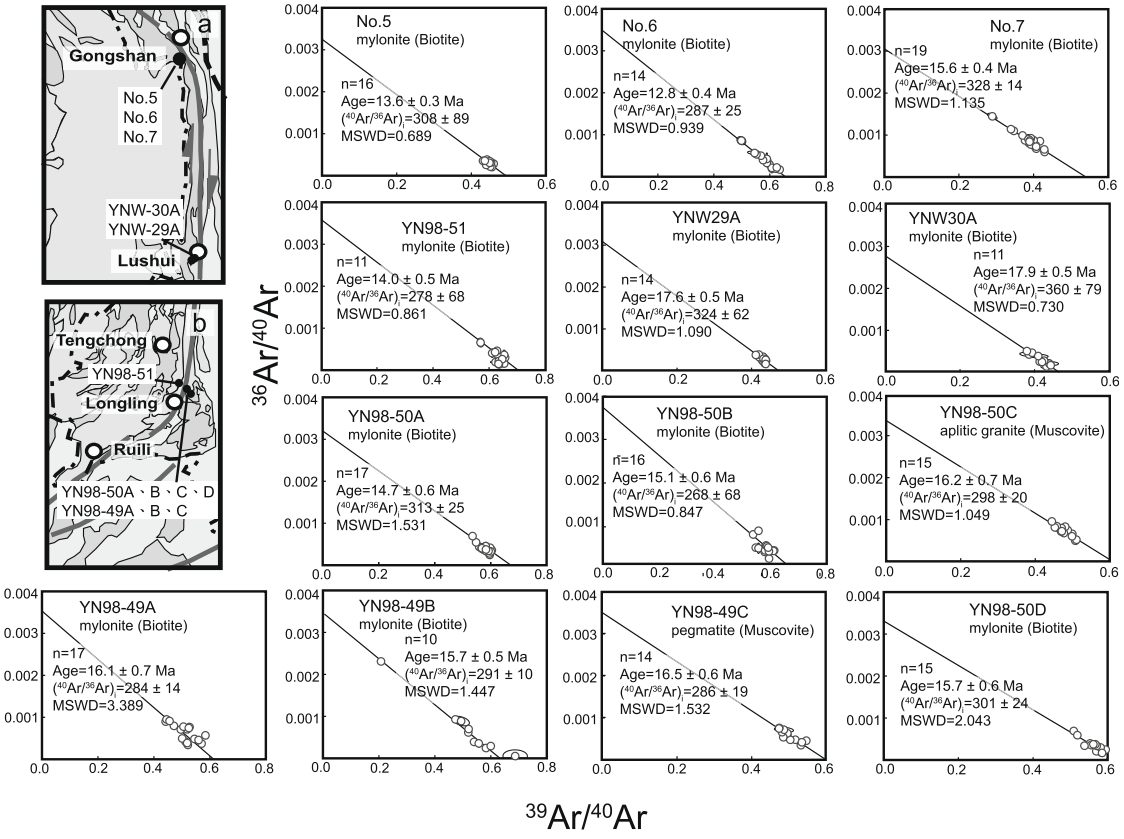

Fig. 7. $^{36}Ar/^{40}Ar$ versus $^{39}Ar/^{40}Ar$ isotope correlation diagrams for samples from the Gaoligong shear zone. Data are represented by open circles, with $\pm 1\sigma$ error ellipses.

5. Discussion

5.1. Deformation history

Shearing along large fault zones has the potential to induce the exhumation and thermal disturbance of deep crustal rocks. Thus, the radiogenic isotopic systems of certain minerals in such rocks could record exhumation and/or cooling events and provide age constraints on faulting activity (e.g., Lacassin et al., 1997; Wang et al., 1998; Lee et al., 2003). In the following sections, we discuss the deformation histories of the Jiali and Gaoligong shear zones with reference to a T-t diagram (Fig. 8) constructed based on the results of this study and age data obtained in previous studies using various dating methods (Ding et al., 2001; Lee et al., 2003; Chung, 2006; Song et al., 2007; Liang et al., 2008).

5.1.1. The Jiali shear zone

A zircon U–Pb age of ~22 Ma obtained for a syn- or pre-kinematic leucogranite (sample ET014B) may constrain the timing of the initiation of shearing along the Jiali Fault in the Tungmai area, where metamorphic complexes record rapid cooling during 22–21 Ma (Fig. 8a). This cooling may reflect a major episode of rapid exhumation in the Tungmai-Bomi area, followed by episodic deformation until 11 Ma. A subsequent rapid cooling event indicated by fission track dates may have been associated with the Late Miocene uplift of the EHS (Chung, 2006). Age data from the Chayu-Shama area (Fig. 1) suggest a similar thermal history, involving rapid cooling from 21 to 15 Ma and a subsequent cooling episode starting at ~10 Ma (Fig. 8b).

The above data indicate that the main phase of deformation along the entire Jiali shear zone started at ca. 22–21 Ma. Along the Tungmai-Bomi section of the north Jiali shear zone, shearing and associated thrusting may have been long-lasting, continuing until 11 Ma (Fig. 8a). This prolonged activity may be attributed to a high geothermal gradient in the area due to shearing or heat advection (Leloup et al., 1999), which possibly induced rapid local cooling following the cessation of deformation or spatially heterogeneous cooling along the shear zone. Such heterogeneity may explain the variable ages obtained for samples from different locations along the Jiali shear zone. Nevertheless, the present thermochronological data suggest that the main phase of deformation along the Jiali shear zone started as early as the Early Miocene (~22 Ma), and was succeeded by a second period of rapid exhumation from ~10 Ma.

5.1.2. The Gaoligong shear zone

Fig. 8c summarizes the radiometric data available for the Gaoligong shear zone, including the U–Pb ages of magmatic zircons that constrain the intrusion age of the protolith (Song et al., 2007; Liang et al., 2008), and $^{40}Ar/^{39}Ar$ ages (this study) of micas that reveal the timing of metamorphism. In combination with the known closure temperatures of the zircon U–Pb and mica K–Ar isotopic systems, these age data suggest rapid cooling for the metamorphic complex in the Gaoligong shear zone, starting at ca. 18 Ma. This date coincides with the period when convergence between India and Eurasia became oblique, resulting in the development of E–W compressional stress in the region east of the Indian indenter (Lee and Lawver, 1995). Therefore, the initiation of oblique convergence may have been related to or induced by dextral shearing along the Gaoligong shear zone, which, in association with thrusting, was most active during the Middle Miocene.

5.2. Tectonic interpretations

As stated above, most of the Cenozoic shear zones in Southeast Asia formed in response to collision between the Eurasia and India

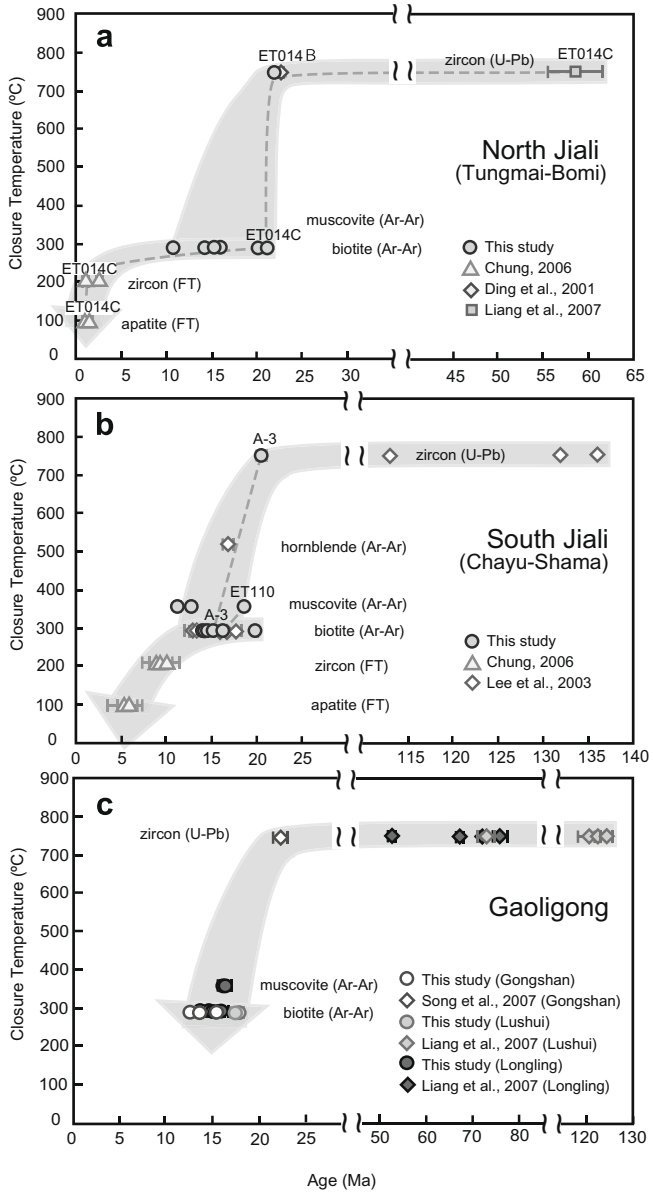

Fig. 8. Cooling paths of deformed granites and mylonites from (a) the northern Jiali shear zone, (b) southern Jiali shear zone, and (c) Gaoligong shear zone. Age data include $^{40}Ar/^{39}Ar$ dates obtained for amphibole, biotite, and muscovite separates (Lee et al., 2003; this study), U–Pb zircon dates (Ding et al., 2001; Lee et al., 2003; Song et al., 2007; Liang et al., 2008), and fission track dates for zircon and apatite (Chung, 2006). Closure temperatures are taken from Parrish (2001).

plates. For example, the sinistral ASRR and dextral Sagaing shear zones are widely considered to represent the major deformation boundaries of the southeastward extrusion of Indochina resulting from the northward indentation of India (Tapponnier et al., 1982). Consequently, the initiation of shearing was broadly synchronous in the ASRR and Sagaing shear zones during the Late Oligocene (Wang et al., 1998, 2000; Bertrand et al., 2001; Leloup et al., 2001; Gilley et al., 2003). Moreover, in both shear zones the main phase of shearing deformation took place at ~22 Ma (Searle, 2006, 2007), with subsequent activity lasting until the mid-Miocene.

Fig. 9 shows all the thermochronological data available for the major shear zones around the EHS. The Jiali shear zone records active shearing from as early as ~22 Ma (Early Miocene), preceding the initiation of movement along the Gaoligong shear zone (~18 Ma) but corresponding to the onset of the main sinistral shearing along the ASRR shear zone (Searle, 2006). Based on these data, in combination with the structural observations described above (i.e., a temporal change in shear sense within the Jiali shear zone from sinistral to dextral), we argue that the initial sinistral shearing recorded along the Jiali shear zone was associated with shearing along the ASRR shear zone, which represented the northern boundary of the southeastward extrusion of Indochina (Fig. 9).

In contrast to the ASRR shear zone, along which sinistral motion ceased at ~18 Ma, deformation in the Jiali shear zone not only continued but also changed to dextral offset, possibly related to movement along the Gaoligong shear zone to the south (Figs. 2 and 9). This change in shear sense is attributed to the ongoing northward indentation of India, which led to eastward movement of the northern Tibetan block and then the clockwise rotation of crustal fragments around the EHS, as suggested by recent GPS-based studies (Chen et al., 2000; Wang et al., 2001; Zhang et al., 2004). The sequence of events depicted in Fig. 9 can therefore be summarized as follows: (1) the Indochina block was extruded southeastward along the sinistral Jiali and ASRR shear zones during the Early Miocene (starting from the Late Oligocene?); and (2) from ca. 18 Ma, crustal deformation around the EHS intensified and movement along the Jiali shear zone changed from sinistral to dextral, linking to the south with the Gaoligong shear zone to act as a bounding structure to the region of clockwise block rotation.

5.3. Implications for Miocene tectonics

The above tectonic interpretation, linking the Jiali and ASRR shear zones in the Early Miocene, needs to account for ~600 km of sinistral offset along the shear zones (Chung et al., 1997), or perhaps even more (Leloup et al., 2001), and geologic correlations. Both of these factors are related to plate reconstructions; however, such reconstructions are difficult to achieve in the Three Rivers area because the tectonic framework has been drastically altered by India–Eurasia collision. Many workers (e.g., Leloup et al., 2001; Akciz et al., 2008) have identified the northwestward extension of the ASRR shear zone by following the plate boundary, thereby extending it to the Bangong–Nujiang suture that separates the Lhasa and Qiangtang terranes in Tibet. We argue against this interpretation because the ASRR does not follow the plate boundary (i.e., the Song Ma suture between the South China and Indochina blocks); instead, it transects the South China block (cf. Chung et al., 1997).

In the eastern Lhasa terrane, the Jiali shear zone occurs entirely within the voluminous Transhimalayan or Gangdese-related batholiths (Fig. 1). The lack of offset markers in this region, combined with the temporal change in shear sense recorded along the shear zone, makes it difficult to determine the amount of strike-slip offset; however, estimates can be made based on regional geologic maps and relevant information such as the nature of initial sinistral shear. If the Jiali shear zone is connected to the ASRR shear zone, it would have cut across at least two sutures: the Bangong–Nujiang in the north and the Nan-Uttaradit in the south. These sutures are equivalent to the Changning–Mengliang and Jinsha sutures, respectively, forming a piercing point in the Three Rivers area that bridges the Indochina block and the Qiangtang terrane. The regional tectonic framework must have been different in the early Cenozoic compared with the present-day, because the space created behind the Indochina block during its southward extrusion would have been filled via the reorganization of crustal blocks and crustal shortening driven by continued indentation of the Indian plate. Given the present state of knowledge, it remains impossible to assess the exact magnitude of southward extrusion and resulting deformation; this uncertainty hampers any direct geologic correlations across the region. Additional detailed investigations are required to solve this problem.

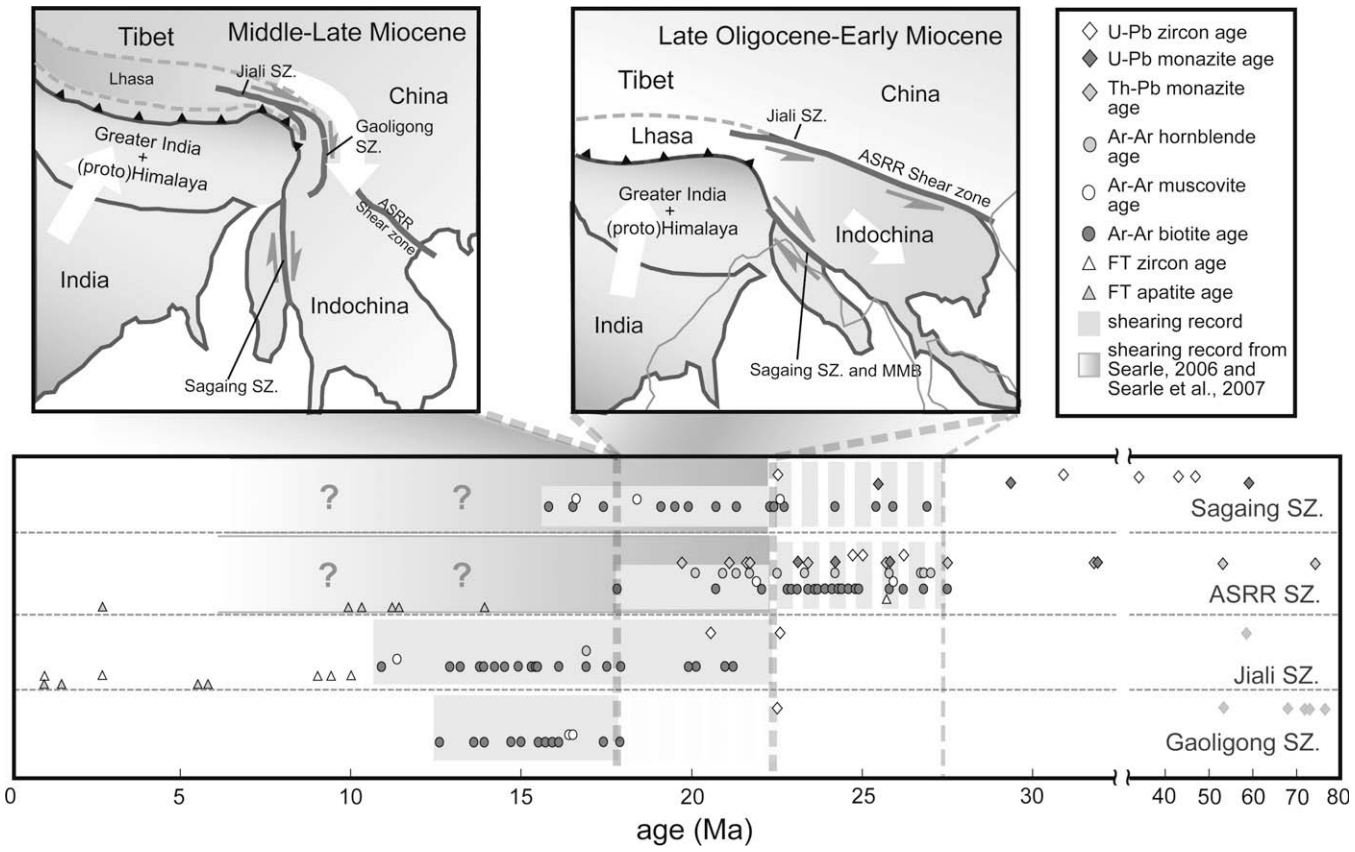

Fig. 9. Summary of the geochronological data available for the Jiali shear zone (Ding et al., 2001; Lee et al., 2003; Chung, 2006; Liang et al., 2008; this study), Gaoligong shear zone (Chung, 2006; Liang et al., 2008; Song et al., 2007; this study), ASRR shear zone (Schärer et al., 1990; Harrison et al., 1992; Leloup et al., 1993; Schärer et al., 1994; Harrison et al., 1996; Wang et al., 1998; Zhang and Schärer, 1999; Wang et al., 2000; Leloup et al., 2001; Gilley et al., 2003; Searle, 2006), and Sagaing shear zone (Bertrand et al., 2001; Barley et al., 2003; Searle et al., 2007). The upper sketch diagrams show the major shear zones and their shear senses during the Late Oligocene to Early Miocene (upper right) and Middle–Late Miocene (upper left).

Temporal changes in the drainage system in Southeast Asia appear to be related to the deformation histories of the principal shear zones in the region. Clark et al. (2004) and Clift et al. (2004) suggested that prior to the Miocene, the Yarlu Tsangpo and other major Tibetan rivers had once linked with the Red River, forming a paleo-Red River system that drained southeastward into the South China Sea. Adopting the argument for major uplift in southern Tibet during the Late Oligocene (Chung et al., 2005), Liang et al. (2008) proposed that this paleo-drainage system developed during the Late Oligocene, with the Yarlu Tsangpo following the path of the Jiali shear zone (Fig. 9).

A subsequent reorganization of regional river patterns occurred in response to the northward migration of the Indochina rivers (cf. Brookfield, 1998) such as the Irrawaddy, which captured the southeastward-flowing Yarlu Tsangpo during the Middle Miocene (Liang et al., 2008), when the Jiali shear zone turned to the south to link with the Gaoligong and Sagaing shear zones (Fig. 9). These scenarios, if correct, highlight the importance of Tibetan uplift and regional topographic changes in terms of both the transformation of the principal shear patterns and the development of the eastern Himalayan river system around the EHS.

6. Concluding remarks

New geochronological data indicate that the major period of shearing along the Jiali and Gaoligong shear zones occurred during ~22–11 and ~18–13 Ma, respectively. Activity along the Jiali shear zone involved an early phase of sinistral movement and a later phase of dextral movement. The early phase can be correlated with Early Miocene (~22–18 Ma) sinistral movement upon the ASRR shear zone, which represented the northern boundary of the southeastward extrusion of the Indochina continent, related to India–Eurasia collision. In contrast, the later dextral phase was associated with the Gaoligong shear zone, which became active at ~18 Ma, forming the deformation boundary around the EHS that confined the clockwise rotation of the extruding Tibet block.

Acknowledgements

This study benefited from financial support by the National Science Council, Taiwan. We thank Prof. Clark Burchfiel and the Editor, Prof. Bor-ming Jahn, for constructive reviews of the manuscript, which led to significant improvements.

References

Akciz, S., Burchfiel, B.C., Crowley, J.L., Yin, J., Chen, L., 2008. Geometry, kinematics, and regional significance of the Chong Shan shear zone, Eastern Himalayan Syntaxis, Yunnan, China. Geosphere 4 (1), 292–314.

Armijo, R., Tapponnier, P., Han, T.-L., 1989. Late Cenozoic right-lateral strike-slip faulting in southern Tibet. Journal of Geophysical Research 94 (B3), 2787–2838.

Barley, M.E., Pickard, A.L., Zaw, K., Rak, P., Doyle, M.G., 2003. Jurassic to Miocene magmatism and metamorphism in the Mogok metamorphic belt and the India-Eurasia collision in Myanmar. Tectonics 22(3), doi:10.1029/2002TC001398.

Bertrand, G., Rangin, C., Maluski, H., Bellon, H., GIAC Scientific Party, 2001. Diachronous cooling along the Mogok Metamorphic belt (Shan scarp, Myanmar): the trace of the northward migration of the Indian syntaxis. Journal of Asian Earth Sciences 19 (5), 649–659.

Brookfield, M.E., 1998. The evolution of the great river systems of southern Asia during the Cenozoic India–Asia collision: rivers draining southward. Geomorphology 22 (3–4), 285–312.

Burchfiel, B.C., 2004. New Technology: New Geological Challenges. GSA Today 14 (2), 4–10. doi:10.1130/1052-5173(2004)014<0004:NTNGC>2.0.CO:2.

Chen, Z., Burchfiel, B.C., Liu, Y., King, R.W., Royden, L.H., Tang, W., Wang, E., Zhao, J., Zhang, X., 2000. Global positioning system measurements from eastern Tibet and their implications for India/Eurasia intercontinental deformation. Journal of Geophysical Research 105 (B7), 16215–16227.

Chu, M.-F., Chung, S.-L., Song, B., Liu, D., O'Reilly, S.Y., Pearson, N.J., Ji, J., Wen, D.-J., 2006. Zircon U–Pb and Hf isotope constraints on the Mesozoic tectonics and crustal evolution of southern Tibet. Geology 34 (9), 745–748.

Chung, L., 2006. Fission track ages as evidence for the thermal history of Jiali fault (Eastern Tibet) and its tectonic implications, M.S. thesis. National Taiwan Univ., Taipei, July, 69 pp.

Chung, S.-L., Lee, T.-Y., Lo, C.-H., Wang, P.-L., Chen, C.-Y., Nguyen, T.Y., Tran, T.H., Wu, G., 1997. Intraplate extension prior to continental extrusion along the Ailao Shan-Red River shear zone. Geology 25 (4), 311–314.

Chung, S.-L., Chu, M.-F., Zhang, Y., Xie, Y., Lo, C.-H., Lee, T.-Y., Lan, C.-Y., Li, X., Zhang, Q., Wang, Y., 2005. Tibetan tectonic evolution inferred from spatial and temporal variations in post-collisional magmatism. Earth-Science Review 68, 173–196. doi:10.1016/j.earscirev.2004.05.001.

Clark, M.K., Schoenbohm, L.M., Royden, L.H., Whipple, K.X., Burchfiel, B.C., Zhang, X., Tang, W., Wang, E., Chen, L., 2004. Surface uplift, tectonics, and erosion of eastern Tibet from large-scale drainage patterns. Tectonics 23, TC1006. doi:10.1029/2002TC001402.

Clift, P.D., Layne, G.D., Blusztajn, J., 2004. The erosional record of Tibetan uplift in the East Asian marginal seas. In: Clift, P.D., Wang, P., Hayes, D., Kuhnt, W. (Eds.), Continent–Ocean Interactions in the East Asian Marginal Seas. AGU, pp. 255–282.

Ding, L., Zhong, D., 1992. Deformation Age for Miocene Right-Lateral Movement along the Gaoligong Strike-Slip Fault, Western Yunnan, Memoir of Lithospheric Tectonic Evolution Research (I), Institute of Geology, Chinese Academy of Science Seismology, pp. 68–73.

Ding, L., Zhong, D., Yin, A., Kapp, P., Harrison, T.M., 2001. Cenozoic structural and metamorphic evolution of the eastern Himalayan syntaxis (Namche Barwa). Earth and Planetary Science Letters 192, 423–438.

Gilley, L.D., Harrison, T.M., Leloup, P.H., Ryerson, F.J., Lovera, O., Wang, J.-H., 2003. Direct dating of left-lateral deformation along the Red River shear zone, China and Vietnam. Journal of Geophysical Research 108 (B2), 2127. doi:10.1029/2001JB001726.

Harrison, T.M., Chan, W., Leloup, P.H., Ryerson, F.J., Tapponnier, P., 1992. An early Miocene transition in deformation regime within the Red River fault zone, Yunnan, and its significance for Indo-Asian tectonics. Journal of Geophysical Research 97 (B5), 7159–7182.

Harrison, T.M., Leloup, P.H., Ryerson, F.J., Tapponnier, P., Lacassin, R., Chen, W., 1996. Diachronous initiation of transtension along the Ailao Shan-Red River shear zone, Yunnan and Vietnam. In: Yin, A., Harrison, T.M. (Eds.), The Tectonic Evolution of Asia. Cambridge University Press, pp. 208–225.

Hodges, K.V., Spear, F.S., 1982. Geothermometry, geobarometry and Al_2SiO triple point at Mt. Oosilauke, New Hampshire. The American mineralogist 67, 1118–1134.

Holdaway, M.J., 1971. Stability of andalusite and the aluminium silicate phase diagrams. American Journal of Science 271, 97–131.

Lacassin, R., Maluski, H., Leloup, P.H., Tapponnier, P., Hinthong, C., Siribhakdi, K., Shuaviroj, S., Sharoenravat, A., 1997. Tertiary diachronic extrusion and deformation of western Indochina: structural and $^{40}Ar/^{39}$ Ar evidence from NW Thailand. Journal of Geophysical Research 102 (B5), 10013–10037.

Lee, T.Y., Lawver, L.A., 1995. Cenozoic plate reconstruction of Southeast Asia. Tectonophysics 251 (1–4), 85–138.

Lee, H.-Y., Chung, S.-L., Wang, J.-R., Wen, D.-J., Lo, C.-H., Yang, T.-Y.F., Xie, Y., Lee, T.-L., Wu, G., Ji, J., 2003. Miocene Jiali faulting and its implications for Tibetan tectonic evolution. Earth and Planetary Science Letters 205, 185–194.

Leloup, P.H., Harrison, T.M., Ryerson, F.J., Chen, W., Li, Q., Tapponnier, P., Lacassin, R., 1993. Structural, petrological, and thermal evolution of a Tertiary ductile strike-slip shear zone: The Ailao Shan-Red River (P.R.C.). Earth and Planetary Science Letters 118, 213–234.

Leloup, P.H., Richard, Y., Battaglial, J., Lacassin, R., 1999. Shear heating in continental strike-slip shear zones: model and field examples. Geophysical Journal International 136, 19–40.

Leloup, P.H., Arnaud, N., Lacassin, R., Kienast, J.R., Harrison, T.M., Phan Trong, T., Replumaz, A., Tapponnier, P., 2001. New constraints on the structure, thermochronology, and timing of the Ailao Shan-Red River shear zone, SE Asia. Journal of Geophysical Research 106 (B4), 6683–6732.

Liang, Y.-H., Chung, S.L., Liu, D., Xu, Y., Wu, F.-Y., Yang, J.-H., Wang, Y., Lo, C.-H., 2008. Detrital zircon evidence for reorganization of the eastern Himalayan river system. American Journal of Science 308, 618–638.

Lo, C.-H., Howard, K.T., Chung, S.-L., Meffre, S., 2002. Laser fusion ^{40}Ar–^{39}Ar ages of Darwin impact glass. Meteoritics and Planetary Science 37, 1555–1562.

Molnar, P., Deng, Q., 1984. Faulting associated with large earthquakes and the average rate of deformation in central and eastern Asia. Journal of Geophysical Research 89 (B7), 6203–6227.

Molnar, P., Tapponnier, P., 1978. Active tectonics of Tibet. Journal of Geophysical Research 83 (B11), 5361–5375.

Ni, J., York, J.E., 1978. Late Cenozoic tectonics of Tibetan Plateau. Journal of Geophysical Research 83 (B11), 5377–5384.

Odin, G.S., 35 collaborators, 1982. Interlaboratory standards for dating purposes. In: Odin, G.S. (Ed.), Numerical Dating in Stratigraphy. United Kingdom, pp. 123–149.

Parrish, R.R., 2001. The response of mineral chronometers to metamorphism and deformation in orogenic belts. In: Miller, J.A., Holdsworth, R.E., Buick, I.S., Hand, M. (Eds.), Continental Reactivation and Reworking. The Geological Society of London, pp. 289–301.

Renne, P.R., Swisher, C.C., Deino, A.L., Karner, D.B., Owens, T.L., DePaolo, D.J., 1998. Intercalibration of standards, absolute ages and uncertainties in $^{40}Ar/^{39}Ar$ dating. Chemical Geology 149, 117–152.

Schärer, U., Tapponnier, P., Lacassin, R., Leloup, P.H., Zhong, D., Ji, S., 1990. Intraplate tectonics in Asia: A precise age for large-scale Miocene movement along the Ailao Shan-Red River Shear Zone. Earth and Planetary Science Letters 97, 65–77.

Schärer, U., Zhang, L.-C., Tapponnier, P., 1994. Duration of strike-slip movements in a large shear zone: the Red River belt, China. Earth and Planetary Science Letters 126, 379–397.

Searle, M.P., 2006. Role of the Red River Shear zone, Yunnan and Vietnam, in the continental extrusion of SE Asia. Journal of the Geological Society 163, 1025–1036.

Searle, M.P., Noble, S.R., Cottle, J.M., Waters, D.J., Mitchell, A.H.G., Hlaing, T., Horstwood, M.S.A., 2007. Tectonic evolution of the Mogok metamorphic belt, Burma (Myanmar) constrained by U-Th-Pb dating of metamorphic and magmatic rocks. Tectonics 26 (3), TC3014. doi:10.1029/2006TC002083.

Song, S.G., Ji, J.Q., Wei, C.J., Su, L., Zheng, Y.D., Song, B., Zhang, L.F., 2007. Early Paleozoic granite in the Nujiang River of northwest Yunnan in southwestern China and its tectonic implications. Chinese Science Bulletin 52 (17), 2402–2406.

Tapponnier, P., Peltzer, G., Armijo, R., Le Dain, A.-Y., Cobbold, P., 1982. Propagating extrusion tectonics in Asia: New insights from simple experiments with plasticine. Geology 10, 611–616.

Wang, E., Burchfiel, B.C., 1997. Interpretation of Cenozoic Tectonics in the right-lateral accommodation zone between the Ailao Shan Shear Zone and the Eastern Himalayan Syntaxis. International Geology Review 39, 191–219.

Wang, P.-L., Lo, C.-H., Lee, T.-Y., Chung, S.-L., Lan, C.-Y., Yem, N.T., 1998. Thermochronological evidence for the movement of the Ailao Shan-Red River shear zone: a perspective from Vietnam. Geology 26, 887–890.

Wang, P.-L., Lo, C.-H., Lee, T.-Y., Chung, S.-L., Lan, C.-Y., Thang, T.V., 2000. Onset timing of left-lateral movement along the Ailao Shan-Red River shear zone: $^{40}Ar/^{39}Ar$ dating constraint from the Nam Dinh Area, northeastern Vietnam. Journal of Asian Earth Sciences 18, 281–292.

Wang, Q., Zhang, P.Z., Freymueller, J.T., Bilham, R., Larson, K.M., Lai, Xi'an, You, X., Niu, Z., Wu, J., Li, Y., Liu, J., Yang, Z., Chen, Q., 2001. Present-day crustal deformation in China constrained by Global Positioning System measurements. Science 294, 574–577.

Zhang, L.S., Schärer, U., 1999. Age and origin of magmatism along the Cenozoic Red River shear belt, China. Contributions to Mineralogy and Petrology 134, 67–85.

Zhang, P.L., Shen, Z., Wang, M., Gan, W., Burgmann, R., Molnar, P., Wang, Q., Niu, Z., Sun, J., Wu, J., Sun, H., You, X., 2004. Continuous deformation of the Tibetan Plateau from global positioning system data. Geology 32, 809–812.

Zhong, D., Wang, Y., Ding, L., 1991. The Tertiary Gaoligong intracontinental strike-slip fault and its associated extensional structure in western Yunnan, China. In: Zhang, X. (Ed.), Annual report 1989–1990 of Division of Lithosphere Tectonic Evolution. Institute of Geology and Geophysics Chinese Academy of Sciences, pp. 18–22.